

## Synthesis, Crystal Structure, and Activity of Pyrazole-Based Inhibitors of p38 Kinase

Matthew J. Graneto,\* Ravi G. Kurumbail,† Michael L. Vazquez, Huey-Sheng Shieh,† Jennifer L. Pawlitz,†,§ Jennifer M. Williams,† William C. Stallings,†,§ Lifeng Geng,§ Ashok S. Narayan,§ Francis J. Koszyk,§ Michael A. Stealey,§ Xiangdong D. Xu,§ Richard M. Weier,§ Gunnar J. Hanson,§ Robert J. Mourey,‡ Robert P. Compton,‡ Stephen J. Mnich,‡ Gary D. Anderson,‡ Joseph B. Monahan,‡ and Rajesh Devraj

Pfizer Global Research & Development, St. Louis Laboratories, 700 Chesterfield Village Parkway, Chesterfield, Missouri 63107

Received October 12, 2006

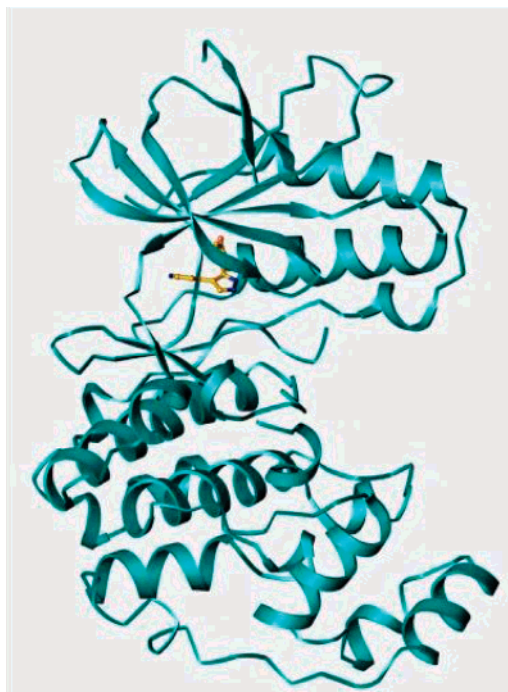
A series of pyrazole inhibitors of p38 mitogen-activated protein (MAP) kinase were designed using a binding model based on the crystal structure of **1** (SC-102) bound to p38 enzyme. New chemistry using dithietanes was developed to assemble nitrogen-linked substituents at the 5-position of pyrazoles. Calculated log *D* was used in tandem with structure-based design to guide medicinal chemistry strategy and improve the *in vivo* activity of a series of molecules. The crystal structure of an optimized inhibitor, **4** (SC-806), in complex with p38 enzyme was obtained to confirm the hypothesis that the addition of a basic nitrogen to the molecule induces an interaction with Asp112 of p38 $\alpha$ . A compound identified from this series was efficacious in an animal model of rheumatic disease.

### Introduction

p38 kinase is a member of the mammalian mitogen-activated protein (MAP) kinase family which comprises important signaling molecules that mediate cellular response to extracellular signals such as environmental stress, growth factors, cytokines, and bacterial endotoxins.<sup>1–4</sup> Members of the MAP kinase family are proline-directed serine/threonine kinases that share sequence similarity and conserved structural domains. In addition to the p38 kinase pathway, the MAP kinase superfamily also includes two other parallel pathways: c-Jun amino-terminal kinases (JNKs) and extracellular signal-regulated kinases (ERKs). Four isoforms of p38 have been identified to date: p38 $\alpha$ , p38 $\beta$ , p38 $\gamma$ , and p38 $\delta$ . On the basis of the size of the buried lipophilic pocket at the ATP site, p38 $\alpha$  and p38 $\beta$  kinases form one subgroup while p38 $\gamma$  and p38 $\delta$  kinases segregate as another subgroup.

Ever since the discovery of p38 kinase in mid-90s, the pharmaceutical industry has aggressively pursued it as a target for the development of disease-modifying antirheumatic drugs (DMARDs).<sup>5–9</sup> Cell-based experiments and preclinical studies in animals have clearly demonstrated that inhibition of p38 $\alpha$  kinase results in significant attenuation of the production of tumor necrosis factor alpha (TNF $\alpha$ ) in response to bacterial lipopolysaccharide (LPS) or other stimulants. Moreover, data from early clinical trials in humans have corroborated these preclinical findings.<sup>10</sup>

In this paper, we describe a program to investigate structure–activity relationships of the 5-position of an early lead molecule, **1** (SC-102),<sup>11</sup> with nitrogen-linked substituents. Much of the rationale for these efforts is based on the crystal structure of **1** bound to p38 enzyme (Figure 1). The binding mode of **1** (Figure 2a) was used to determine which of the positions on the molecule might be amenable for further optimization of binding. Our early work employed a 4-fluorophenyl group as shown in **1**; however, structure activity relationships unrelated to this manuscript<sup>12</sup> led to our later work employing a 4-chlorophenyl group to explore the structure–activity relationships of the



**Figure 1.** Ribbon diagram of p38 $\alpha$  complexed with **1**. The inhibitor is bound at the ATP binding site located at the hinge region between the two lobes of the enzyme. Crystals of p38 $\alpha$  complex were obtained by hanging drop vapor diffusion methods. Diffraction data were measured at the IMCA-CAT beamline at the Advanced Photon Source to 1.65 Å resolution, and the structure has been refined with good agreement between the data and the model ( $R_{\text{free}}$  of 27.9% and  $R_{\text{work}}$ : 25.8%).

5-position of the pyrazole ring. In the process of this exploration, we developed novel chemical methods to assemble 5-aminopyrazoles.

### Chemistry

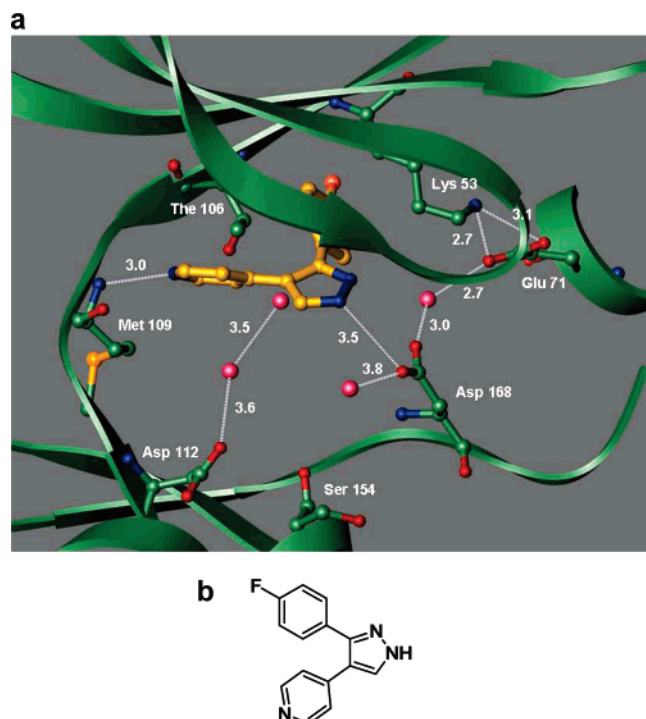
The pyrazole core structures in this paper were constructed by two methods. In our early work, a thiosemicarbazide route<sup>13</sup> was used. When not available commercially, thiosemicarbazides **2**<sup>14</sup> were prepared by reacting an amine with thiophosgene and

\* To whom correspondence should be addressed. Phone: 636-247-7355. Fax: 636-247-2086. E-mail: matthew.j.graneto@pfizer.com.

† Structural and Computational Chemistry.

‡ Biological Sciences.

§ No longer employed by Pfizer.



**Figure 2.** a. Close-up view of the ATP site of **1**/p38 $\alpha$  complex. Interactions of **1** at the ATP site of p38 $\alpha$ . Some of the key side chains of p38 $\alpha$  are displayed (C: green, N: dark blue, O: red, S: yellow, and F: orange). The carbon atoms of the inhibitor are shown in gold color. Some of the key hydrogen bonds are shown as dotted white lines. Some of the bound solvent molecules near the ligand are shown as pink spheres. The pyridyl nitrogen forms a hydrogen bond with the peptide backbone of Met 109 while the central pyrazole interacts with Asp 168. The carbon at C-5 of pyrazole is  $\sim 6.5$  Å away from the side chain of Asp 112. b. Chemical structure of **1**.

hydrazine (Scheme 1). Once prepared, the thiosemicarbazides are then condensed with 2-chloro-1-(4-fluorophenyl)-2-(pyridin-4-yl)ethanone **3**,<sup>15</sup> to produce a pyrazole via cyclocondensation and desulfurization using methods similar to those described by Pfeiffer et al.<sup>16</sup>

Although this method was productively used to make many analogues, it suffers from several faults. First, it uses thiophosgene, which requires special handling. Second, it necessitates the preparation of a thiosemicarbazide of each new desired amine. And more significantly, it often provided poor yields and intractable mixtures. We therefore sought a method that would alleviate some of these problems.

In our initial attempts, a dithioketeneacetal group<sup>17</sup> was installed on 1-(4-fluorophenyl)-2-(4-pyridyl)ethanone, **5**. The thiomethyl groups were then displaced by thiomorpholine to produce a ketene aminal, **7**. With this intermediate in hand, we expected nucleophilic hydrazine to condense with the keto group of the ketene aminal compound **7** and then do an intramolecular displacement of one of the amines to complete the cyclization to the pyrazole (Scheme 2, upper path). Much to our surprise, the ketene aminal compound **7** was inert to hydrazine under a variety of conditions including high temperatures, extended reaction times, or refluxing in neat hydrazine hydrate and did not produce the desired pyrazole.

In the course of our experiments, we discovered some desired product was formed in very low yield. We postulated that the pyrazole product arose from incomplete formation of the ketene aminal compound **7**. The thioamide compound **8**, carried on as an impurity, was responsible for all of the pyrazole formation (Scheme 2, lower path).

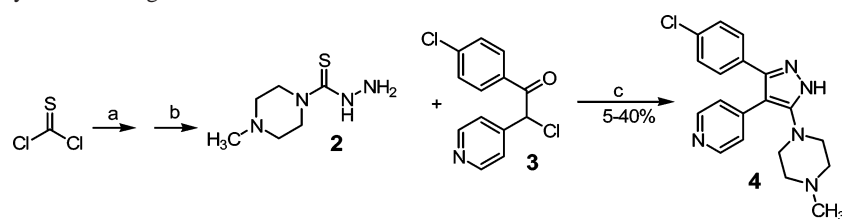
We then sought a way to reliably prepare thioamide compounds of our template. Several attempts to modify the conditions of step b in Scheme 2 to produce more of the thioamide resulted in complex mixtures and ketene aminal formation. Finally, a new method that could cleanly prepare thioamides of our template was found. We discovered that by tying the thiomethyl groups of compound **6** together to form a dithietane<sup>17,18</sup> ring, the product **10** would cleanly react with 1 equiv of a secondary amine to produce the necessary thioamides **11** (Scheme 3). Further, not only could dithietanes be cleanly prepared on our template, but purified thioamide compounds would condense with hydrazine to produce the desired pyrazoles in good yield (Scheme 3). This new procedure was scalable and could be routinely carried out without chromatography.

## Biological Results and Discussion

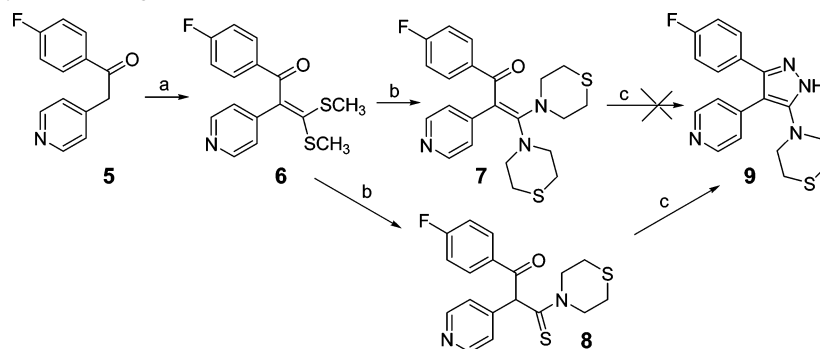
Our earlier work had identified **1** as a moderately potent inhibitor of p38 MAP kinase (p38 enzyme IC<sub>50</sub> = 600 nM, log *D* @ pH 7 = 1.4, LPS-induced TNF production in rat (rLPS) % inhibition @ 20 mpk = 90).<sup>12</sup> With an inhibitor-bound X-ray structure of p38 enzyme in hand, we used **1** as a new lead for further improvement. The inhibitor **1** has two aromatic groups attached to a central pyrazole template. Analysis of our crystal structure (Figures 1 and 2a) showed that the 4-fluorophenyl group is bound in a deep lipophilic pocket of the enzyme, completely shielded from the solvent. The pyridine ring of **1** is enclosed in a hydrophobic pocket of the enzyme formed by residues Val 38, Ala 51, His 107, Leu 108, Met 109, and Leu 167. Moreover, the nitrogen at the 4-position of the pyridine ring accepts a hydrogen bond from the amide nitrogen of Met 109 (3.0 Å). The pyrazole group of **1** serves as a central framework that helps to optimally position the two aromatic groups in the ATP binding site of p38 kinase. One edge of the pyrazole moiety is stabilized by interactions with the flexible glycine flap (residues 31–36) that contains the consensus motif, Gly-X-Gly-X-X-Gly where X is any amino acid.<sup>19</sup> In addition, one of the nitrogen atoms of the pyrazole ring directly interacts (3.5 Å) with the carboxylate of Asp 168. However, the 5-position of the pyrazole ring is not involved in any key interactions. Substitution of this 5-position should have the correct trajectory to place substituents in the unoccupied solvent region that could help to improve the physical properties of the inhibitors. Moreover, the molecular electrostatic surface (Figure 3) indicates that a basic substituent appended to the 5-position might also contribute to enhancing the potency by directly engaging with the side chain of Asp 112.

While carbon-, oxygen-, and sulfur-linked substituents were also investigated, this paper is focused on nitrogen-linked substituents at the 5-position. First, we wanted to choose groups for inclusion at the 5-position that were large enough to fill the available space. We felt that by sweeping water out of the pocket, a tighter binding inhibitor could be found.<sup>20–22</sup> A variety of lipophilic groups were prepared as shown in Table 1. Compounds **12–16** demonstrate that large lipophilic groups are tolerated by the enzyme. While these compounds show a modest increase in potency over the initial lead **1**, this did not translate to antiinflammatory efficacy in an animal model, rLPS. We postulated that this may be due to poor physical properties, such as a high log *D* and low aqueous solubility.<sup>23–25</sup>

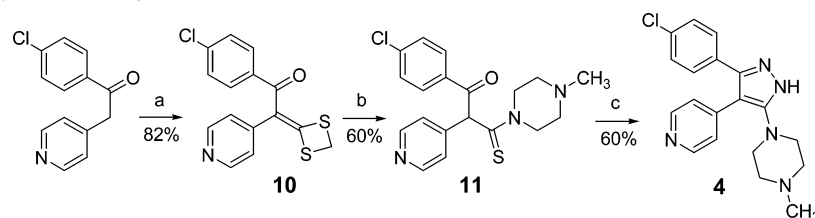
We then prepared a series of compounds with improved physical properties. First, we tried to lower the log *D*, and second we hoped to further increase potency by engaging nearby amino acid residues with hydrogen-bonding potential. A careful examination of the **1** crystal structure (Figure 2a) showed that

Scheme 1<sup>a</sup> Synthesis of Pyrazoles Using Thiosemicarbazide

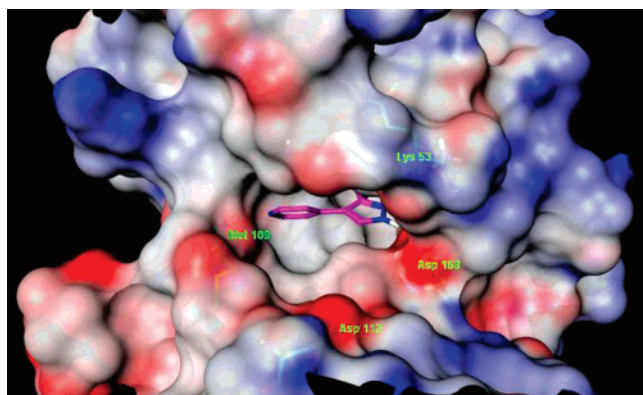
<sup>a</sup> Reagents and conditions: (a) *N*-methylpiperazine, ether,  $-10^{\circ}$ ; (b)  $N_2H_4$ , dropwise in ether; (c) DMF,  $100^{\circ}$

Scheme 2<sup>a</sup> Synthesis of Pyrazoles Using Dithioketeneacetals.

<sup>a</sup> Reagents and conditions: (a) NaH,  $CS_2$ ,  $CH_3I$ ; (b) thiomorpholine, toluene; (c)  $N_2H_4$ .

Scheme 3<sup>a</sup> Synthesis of Pyrazoles Using Dithietanes.

<sup>a</sup> Reagents and conditions: (a)  $CS_2$ ,  $CH_2Br_2$ , acetone,  $K_2CO_3$ ; (b) *N*-methylpiperazine, toluene; (c)  $N_2H_4$ .



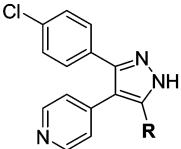
**Figure 3.** Molecular electrostatic surface of 1/p38 $\alpha$  complex. The ligand is shown as a stick figure (C: pink, N: dark blue, H: white, and F: orange). The surface (partially transparent) is color-coded based on the electrostatic charge distribution. Blue represents positive charge and red indicates negative charge. Some of the amino acid residues of p38 are visible through the surface and are labeled. One of the striking features is the presence of an intense, negative charge due to Asp 112 on the C-lobe of the enzyme,  $\sim 6.5$  Å away from the C-5 position of the pyrazole of the inhibitor.

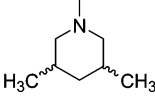
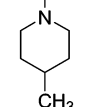
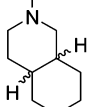
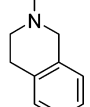
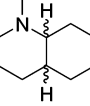
the side-chain carboxylate of Asp 112 is only 6.5 Å away from the 5-position of the pyrazole. We also observed that the main-chain carbonyl oxygen of Ser 154 is pointed toward the 5-position of the pyrazole (6.4 Å).

Compounds **17** and **18** (Table 2) are examples of compounds with a reduced log *D*. While these two compounds are only slightly better than **1** in the *in vitro* assay (3–5 times more

potent), they both show a better correlation between their enzyme activity and antiinflammatory efficacy in the animal model rLPS. Entries **19–21** also have a lower log *D* and improved physical properties. In addition, all three compounds contain a moiety with a basic nitrogen that could potentially interact with Asp 112 of p38 $\alpha$ . A direct comparison of compounds **12** and **13** to compounds **21** and **4**, respectively, (nitrogen for carbon substitution in the piperazine vs piperidine analogues) showed that the piperazine analogues provided an additional increase in enzyme potency accompanied by an increase in *in vivo* antiinflammatory activity. Thus, compounds **19–21** and **4** offer both improved physical properties and greater potency, which is confirmed by the high levels of activity in the *in vivo* antiinflammatory assay.

Our presumption that the basic nitrogen of compounds **19–21** and **4** interacts with the side chain of Asp 112 was confirmed when we solved the crystal structure of **4** complexed with p38 $\alpha$ . As expected, the pyridyl nitrogen interacts with the adenine recognition element in the hinge region while the 4-chlorophenyl group binds in the unique lipophilic pocket of p38 $\alpha$  (Figure 4). The two nitrogen atoms of the central pyrazole form solvent-mediated interactions (2.5–2.8 Å) with the carboxylate of Asp 168. The piperazine ring at the 5-position of the pyrazole extends toward the solvent surface displacing a bound water molecule seen in the crystal structure of **1** (Figure 2a) and forms van der Waals interactions with residues from the glycine-rich loop, hinge region, and the C-lobe of p38 $\alpha$ . The piperazine ring and the pyrazole ring have a torsion angle of  $36^{\circ}$ . The terminal, basic nitrogen of the piperazine ring forms a hydrogen bond to

**Table 1.** 5-Position Lipophilic Substituents<sup>a</sup>


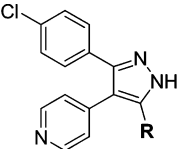
Compd. Number	R	p38 kinase enzyme IC <sub>50</sub> nM	LogD @ pH 7 <sup>b</sup>	rLPS % inh @ 20 mpk <sup>c</sup>
12		130	3.96	53
13		130	3.47	16
14		260	4.52	11
15		190	3.83	12
16		40	4.52	33

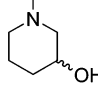
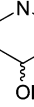
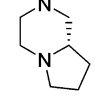
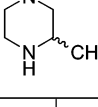
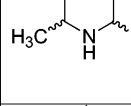
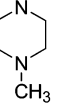
<sup>a</sup> All compounds analyzed C, H, N. <sup>b</sup> Calculated using ACD software. <sup>c</sup> Compounds dosed orally 4 h prior to LPS challenge.

a bound solvent molecule (2.8 Å) which in turn is engaged in an interaction with the Asp 112 side chain (2.8 Å) and main-chain oxygen of Ser 154 (2.6 Å).

Comparison of the crystal structure of **4** with similar imidazole analogues reveals subtle differences in the orientation and location of the substituents from the central heterocyclic rings. For example, Wilson et al.<sup>26</sup> have reported the crystal structure of p38 $\alpha$  kinase complexed with **23** (VK-19911,  $K_d$  = 15 nM) that contains a piperidyl moiety from a central imidazole ring in an analogous position to the piperazyl group of **4** (Figure 5a). They observed that the piperidyl group forms a salt bridge with the carboxylate group of Asp 168 and forms van der Waals interactions with the side chains of Met 109 and Leu 167. Similarly, Wang et al.<sup>27</sup> have reported that the piperidine ring in **22** (SB-220025, p38 enzyme IC<sub>50</sub> = 19 nM) forms a hydrogen bond with one of the oxygen atoms of the side-chain carboxylate of Asp 168 in its complex with murine p38 $\alpha$  kinase. **22** is an imidazole-based inhibitor that contains 2-aminopyrimidine as the hinge-region recognition element (Figure 5a). Similar to **23**, the piperidine ring in **22** also forms an edge-to-face interaction with the side chain of Tyr 35 from the flexible glycine loop.

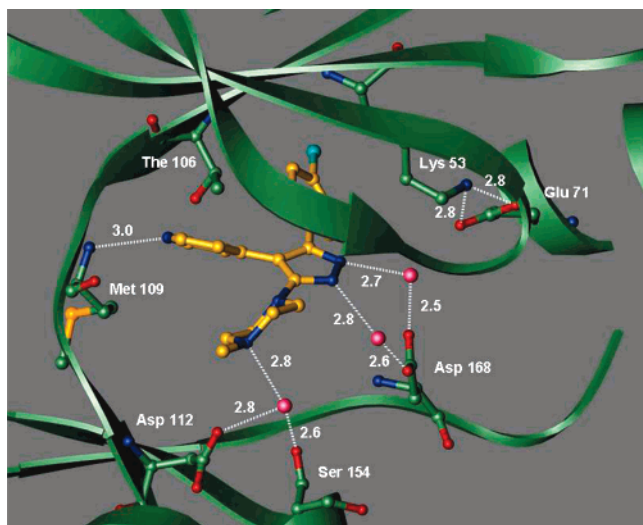
Superposition of the crystal structures of p38 complexed with **4** and **22** (PDB accession code 1BL7) clearly show the different locations of the piperazyl and piperidyl substituents in the two

**Table 2.** 5-Position Substituents with Lower Log D<sup>a</sup>


Compd. #	R	p38 kinase enzyme IC <sub>50</sub> nM	LogD @ pH 7 <sup>b</sup>	rLPS % inh @ 20, 5 mpk <sup>c</sup>
17		190	1.24	75, nd
18		110	1.31	91, 52
19		62	1.33	89, nd
20		16	0.60	95, 84
21		12	1.07	96, 93
4		50	1.15	95, 98

<sup>a</sup> All compounds analyzed C, H, N. <sup>b</sup> Calculated using ACD software. <sup>c</sup> Compounds dosed orally 4 h prior to LPS challenge.

compounds (Figure 5a). The two structures were overlaid using a cluster of 13 C $\alpha$  atoms distributed around the ligand binding site to minimize artifacts that arise during usual superposition of kinase structures. The aromatic rings of the two inhibitors do not superimpose exactly on each other because of subtle conformational differences in the ATP site of the two complexes. As a result, the piperazine group of **4** points in a slightly different trajectory compared with the piperidyl substituent of **22**. Also, there are subtle changes in the conformation of the saturated heterocyclic rings in the two compounds. Consequently, the piperazyl nitrogen substituted by the methyl group of **4** is located significantly closer to the side-chain carboxylate of Asp 112 (3.5 Å) than to that of Asp 168 (7.7 Å). In contrast, the piperidine nitrogen of **22** forms a hydrogen-bonding interaction with the carboxylate of Asp 168, similar to that observed in the structure of **23**.<sup>26</sup> These structural differences illustrate that although the imidazole-based inhibitors (**22** and **23**) and the pyrazole-based compounds discussed in this manuscript have similar chemical structures, there are significant differences in their molecular interactions with the target enzyme.



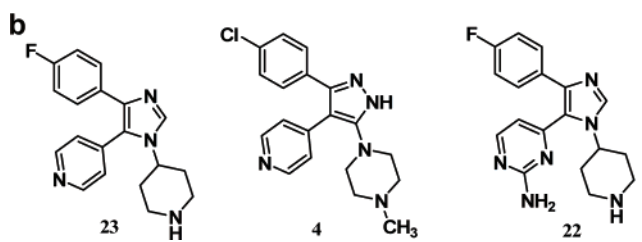
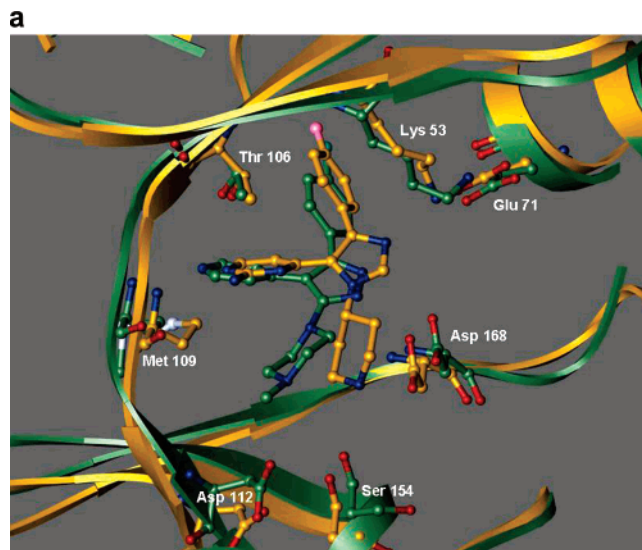
**Figure 4.** Close-up view of **4**/p38 $\alpha$  complex. Interactions of **4** at the ATP site of p38 $\alpha$ . Atoms are colored as in Figure 2a and key hydrogen bonds are shown as dotted white lines. Diffraction data were measured at the IMCA-CAT beamline at the Advanced Photon Source to 1.8 Å resolution, and the structure has been refined with good agreement between the data and the model ( $R_{\text{free}}$  of 27.5% and  $R_{\text{work}}$ : 23.2%). The central pyrazole ring interacts with Asp 168 via two bound solvent molecules. The terminal piperazyl group forms water-mediated interactions with Ser 154 and the side chain of Asp 112.

**In Vivo Efficacy Models.** Compounds with high levels of activity in the p38 MAP kinase enzyme assay<sup>15</sup> were routinely advanced to *in vivo* assays. The rLPS assay data shown in Tables 1 and 2 was generated by ELISA analysis of TNF $\alpha$  from serum samples collected 1.5 h after intravenous LPS challenge of male Harlan Lewis rats. Compound administration was by oral gavage 4 h prior to LPS challenge.<sup>15</sup>

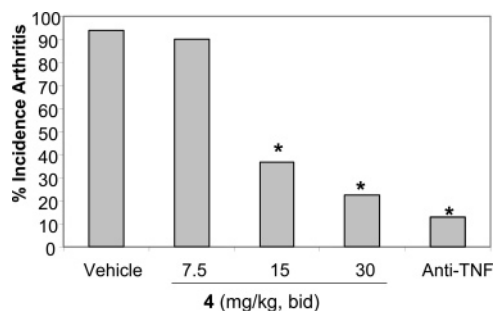
Compound **4**, with an efficacy of 98% @ 5 mpk in the rLPS assay, was advanced to an animal model of rheumatic disease, mouse collagen-induced arthritis (mCIA).<sup>28,29</sup> The mCIA animal model was chosen since the histopathology of joint inflammation is similar to that in human RA, as is the pathogenic role of TNF $\alpha$  and IL-1.<sup>30,31</sup> Arthritis was induced in male DBA/1 mice by subcutaneous injection of type II chick collagen in Freund's adjuvant on days 1 and 21. Compound **4** was administered in Methocel/Tween by oral gavage bid from days 21–56. Anti-TNF antibody<sup>32</sup> was administered ip once a week as a comparator. As shown in Figure 6, both anti-TNF antibody and **4** at 15 and 30 mg/kg significantly decreased incidence of arthritis in animals compared to vehicle treatment with  $p < 0.05$  (Logistical Regression Model). Statistically, there were no differences between animals treated with **4** (30 mg/kg) or anti-TNF antibody.

## Conclusion

A series of compounds were made to explore the structure–activity relationships at the 5-position of pyrazole inhibitors of p38 MAP kinase. New chemistry using dithietanes was discovered to facilitate the exploration of the 5-position with nitrogen-linked substituents. Crystal structure data for **1** was used to determine the binding mode which helped to guide synthesis and elucidation of structure–activity relationships. The compounds disclosed show the progression of improved physical properties and potency leading to **4**, a potent inhibitor of p38 MAP kinase. The binding mode of **4** was confirmed by its crystal structure bound to p38 enzyme, and **4** was shown to suppress disease incidence at 30 mpk in an eight week model of mouse collagen-induced arthritis.



**Figure 5.** a. Overlap of the crystal structures of p38 $\alpha$  complexes with **4** and **22** from ref 27. Some of the key side chains of p38 $\alpha$  are displayed. The carbon atoms of the protein and ligand in the **4** structure are shown in green while those in the **22** structure are shown in gold. Nitrogen atoms in both structures are colored as dark blue, oxygen as red, sulfur as white, chlorine as light blue, and fluorine as pink. The piperidyl group in the **22** structure forms hydrogen-bonding interactions with the carboxylate side chain of Asp 168. In contrast, the piperazyl group in the **4** structure points toward the side chain of Asp 112 and forms water-mediated interactions with the carboxylate side chain of Asp 112 (See Figure 4). b. Chemical structures of **23**, **4**, and **22**.



**Figure 6.** Inhibition of collagen-induced arthritis by **4**. Mice treated between days 21 and 56 with **4** (po bid) or anti-TNF antibody<sup>32</sup> (ip once/week) were evaluated for signs of arthritis. Groups marked with an asterisk were significantly different from vehicle,  $p < 0.05$ , 8–10 animals per group.

## Experimental Section

**General.** All reagents and solvents were of commercial quality and used without further purification. <sup>1</sup>H spectra were recorded using a 300 or 400 MHz Varian NMR spectrometer. Chemical shifts are reported in parts per million relative to an internal standard. Melting points were determined using a Mettler FP81HT automated melting point apparatus and are uncorrected. Microanalyses were performed by Atlantic Microlabs Norcross, GA. Column chromatography was performed on a Biotage preparative liquid chromatography instrument using silica gel columns or on a Gilson HPLC system using a 15  $\mu$ m 100A, C18 column (25 mm ID  $\times$  100 mm

L). Reported yields are not optimized, with emphasis on purity of products rather than quantity.

**4-[3-(4-Fluorophenyl)-1H-pyrazol-4-yl]pyridine (1).** To a suspension of 1-(4-fluorophenyl)-2-(4-pyridyl)ethanone<sup>15</sup> (30 g, 0.14 mol) in THF (50 mL) was added dimethylformamide dimethylacetate (50 mL). The mixture was stirred at room temperature for 48 h, concentrated, and triturated with hexanes (150 mL) to produce a yellow solid which was dissolved in ethanol (125 mL) and cooled to 0 °C. Hydrazine hydrate (12.5 g, 0.25 mol) was added, and the mixture was stirred at room temperature for 3 h. The mixture was concentrated, dissolved in chloroform (200 mL), washed with water (100 mL), and extracted with hydrochloric acid solution (10%, 150 mL). The aqueous extract was treated with activated charcoal (0.5 g) at 70 °C for 10 min, filtered through celite, and neutralized with stirring and external cooling to pH 7–8 with sodium hydroxide (20%). A fine white precipitate was filtered and dried (27.3 g, 91%): mp 207.7–207.8 °C; <sup>1</sup>H NMR (DMSO-*d*<sub>6</sub>/300 MHz) 13.4 (bs, 1H), 8.49 (d, *J* = 2 Hz, 2H), 7.9 (bs, 1H), 7.34 (d, *J* = 4.4 Hz, 2H), 7.27 (m, 2H), 7.16 (m, 2H). Anal. (C<sub>14</sub>H<sub>10</sub>FN<sub>3</sub>) C, H, N.

**1-[5-(4-Chlorophenyl)-4-(4-pyridinyl)-1H-pyrazol-3-yl]-4-methylpiperazine (4).** To a suspension of **11** (52.0 g, 0.14 mol) in 500 mL of dry tetrahydrofuran was added anhydrous hydrazine (8.9 g, 0.28 mol) dropwise. The reaction mixture was stirred at room temperature for 16 h. A pale yellow precipitate was filtered and recrystallized from hot methanol to produce a white powder (30.2 g, 60%): mp 267–268 °C; <sup>1</sup>H NMR (acetone-*d*<sub>6</sub>/300 MHz) 11.8 (br s, 1H), 8.46 (m, 2H), 7.41 (m, 2H), 7.33 (br m, 4H), 2.96 (m, 4H), 2.41 (m, 4H), 2.22 (s, 3H). Anal. (C<sub>19</sub>H<sub>20</sub>ClN<sub>5</sub>) C, H, N.

**1-(4-Fluorophenyl)-3,3-bis(methylthio)-2-pyridin-4-ylprop-2-en-1-one (6).** To 1-(4-fluorophenyl)-2-(4-pyridyl)ethanone<sup>15</sup> (**5**) (1.0 g, 4.7 mmol) in anhydrous THF (10 mL) was added a solution of 1 M potassium tert-butoxide in THF (10 mL, 10 mmol). The reaction mixture was stirred for 15 min at room temperature, and then carbon disulfide (0.31 mL, 5.1 mmol) was added. After several minutes, methyl iodide (0.64 mL, 10.3 mmol) was added and the reaction allowed to stir for 4 h. The reaction mixture was diluted with saturated sodium bicarbonate solution (25 mL) and extracted twice with ethyl acetate (35 mL). The combined ethyl acetate layers were washed with water (25 mL) and brine (25 mL). The organic solution was dried (MgSO<sub>4</sub>), filtered, and concentrated to an orange oil. The oil solidified upon standing (1.4 g, 94%): mp 80.2–82.1 °C; <sup>1</sup>H NMR (CDCl<sub>3</sub>/300 MHz) 8.59 (d, 2H), 7.96 (m, 2H), 7.38 (m, 2H), 7.14 (m, 2H), 2.33 (s, 3H), 2.23 (s, 3H). Anal. (C<sub>16</sub>H<sub>14</sub>FNOS<sub>2</sub>) C, H, N.

**4-[5-(4-Fluorophenyl)-4-pyridin-4-yl-1H-pyrazol-3-yl]thiomorpholine (9).** To **6** in toluene (6 mL) was added thiomorpholine (502 μL, 5 mmol). The reaction mixture was heated between 80 and 110 °C. After about 3 h, 1-(4-fluorophenyl)-2-pyridin-4-yl-3,3-dithiomorpholin-4-ylprop-2-en-1-one (**7**) began to precipitate from the reaction mixture. When the starting material was consumed, the reaction mixture was cooled to room temperature, and the remaining **7** was removed by filtration. To the toluene solution were added hydrazine hydrate (1 mL) and sufficient ethanol to create a homogeneous solution. The reaction mixture was then stirred at room temperature for 3 d. The reaction mixture was diluted with ethyl acetate (50 mL) and extracted twice with water and once with brine (25 mL). The organic solution was dried (MgSO<sub>4</sub>), filtered, and concentrated to a reddish solid. The solid was triturated with acetonitrile, collected by filtration, and dried in vacuo. The dried material was recrystallized from ethanol, acetonitrile, and ethyl acetate to produce a white solid (63 mg, 7%): <sup>1</sup>H NMR (DMSO-*d*<sub>6</sub>/300 MHz) 12.65 (br s, 1H), 8.45 (m, 2H), 7.27 (m, 6H), 3.14 (m, 4H), 2.63 (m, 4H). ESHRMS *m/z* 341 (M + H). ESHRMS *m/z* 341.1241 (M + H, C<sub>18</sub>H<sub>18</sub>FN<sub>4</sub>S requires 341.1236).

**1-(4-Chlorophenyl)-2-(1,3-dithietan-2-ylidene)-2-pyridin-4-ylethanone (10).** To a solution of 1-(4-chlorophenyl)-2-(4-pyridyl)ethanone<sup>15</sup> (70.0 g, 0.3 mol), dibromomethane (200 mL) and carbon disulfide (25.9 g, 0.34 mol) in acetone (800 mL) was added potassium carbonate (83.0 g, 0.6 mol). The reaction mixture was

stirred at room temperature for 24 h. An additional 2 equiv of potassium carbonate and 1 equiv of carbon disulfide was added, and the stirring was continued for another 24 h. Solvent was removed, and the residue was partitioned between dichloromethane and water. The organic layer was washed with brine, dried (MgSO<sub>4</sub>), and filtered. The filtrate was concentrated, and the crude product was stirred with 1 L of a mixture of ethyl acetate and ether (1:9) to give pure product (78.4 g, 82%) as a yellow solid: mp 185.3–185.4 °C; <sup>1</sup>H NMR (acetone-*d*<sub>6</sub>/300 MHz) 8.49 (m, 2H), 7.31 (m, 4H), 7.09 (m, 2H), 4.39 (s, 2H). Anal. (C<sub>15</sub>H<sub>10</sub>ClNOS<sub>2</sub>) C, H, N.

**1-(4-Chlorophenyl)-3-(4-methylpiperazin-1-yl)-2-pyridin-4-yl-3-thioxopropan-1-one (11).** A mixture of **10** (78.3 g, 0.24 mol) and 1-methylpiperazine (75.0 g, 0.73 mol) in toluene (800 mL) was heated to reflux for 2 h. Solvent and excess 1-methylpiperazine was removed under vacuum, and the residue was triturated with a mixture of ethyl acetate and ether (1:3) to give the product as yellow crystals (53.0 g, 60%): mp 149–151 °C; <sup>1</sup>H NMR (acetone-*d*<sub>6</sub>/300 MHz) 8.58 (m, 2H), 7.95 (m, 2H), 7.54 (m, 4H), 6.54 (s, 1H), 4.37 (m, 2H), 4.1 (m, 2H), 3.92 (m, 1H), 2.49 (m, 2H), 2.33 (m, 1H), 2.20 (s, 3H), 1.99 (m, 1H). Anal. (C<sub>19</sub>H<sub>20</sub>ClN<sub>3</sub>OS) C, H, N.

**4-[3-(4-Chlorophenyl)-5-(3,5-dimethylpiperidin-1-yl)-1H-pyrazol-4-yl]pyridine (12).** This compound was prepared using the methods described in the synthesis of **4**, **10**, and **11**. mp 245.7–247.3 °C; <sup>1</sup>H NMR (DMSO-*d*<sub>6</sub>/400 MHz) 8.43 (d, *J* = 6.0 Hz, 2H), 7.43 (d, *J* = 8.8 Hz, 2H), 7.25 (d, *J* = 8.4 Hz, 2H), 7.23 (d, *J* = 6.0 Hz, 2H), 3.08 (br d, *J* = 10.0 Hz, 2H), 2.08 (dd, *J* = 11.6 Hz and *J* = 11.2 Hz, 2H), 1.67 (m, 2H), 0.71 (d, *J* = 6.4 Hz, 6H). ESHRMS *m/z* 367.1689 (M + H, C<sub>21</sub>H<sub>23</sub>ClN<sub>4</sub> requires 367.1693). Anal. (C<sub>21</sub>H<sub>23</sub>ClN<sub>4</sub>) C, H, N.

**4-[3-(4-Chlorophenyl)-5-(4-methylpiperidin-1-yl)-1H-pyrazol-4-yl]pyridine (13).** This compound was prepared using the methods described in the synthesis of **4**, **10**, and **11**. mp 261.1–261.8 °C; <sup>1</sup>H NMR (DMSO-*d*<sub>6</sub>/300 MHz) 11.6 (br s, 1H), 8.47 (m, 2H), 7.46 (m, 2H), 7.28 (m, 4H), 3.16 (d, *J* = 12.0 Hz, 2H), 2.55 (br m, 2H), 1.58 (d, *J* = 11.7 Hz, 2H), 1.43 (br m, 1H), 1.20 (m, 2H), 0.92 (d, *J* = 6.3 Hz, 3H). Anal. (C<sub>20</sub>H<sub>21</sub>ClN<sub>4</sub>) C, H, N.

**2-[3-(4-Chlorophenyl)-4-pyridin-4-yl-1H-pyrazol-5-yl]decahydroisoquinoline (14).** This compound was prepared using the methods described in the synthesis of **4**, **10**, and **11**. mp 231.4–232.7 °C; <sup>1</sup>H NMR (DMSO-*d*<sub>6</sub>/300 MHz) 12.7 (br s, 1H), 8.48 (d, *J* = 5.6 Hz, 2H), 7.45 (d, *J* = 8.4 Hz, 2H), 7.27 (m, 4H), 3.08 (m, 2H), 2.65 (m, 2H), 1.2–1.7 (br m, 10H). ESHRMS *m/z* 393.1851 (M + H, C<sub>23</sub>H<sub>25</sub>ClN<sub>4</sub> requires 393.1846). Anal. (C<sub>23</sub>H<sub>25</sub>ClN<sub>4</sub>) C, H, N.

**2-[3-(4-Chlorophenyl)-4-pyridin-4-yl-1H-pyrazol-5-yl]-1,2,3,4-tetrahydroisoquinoline (15).** This compound was prepared using the methods described in the synthesis of **4**, **10**, and **11**. mp 234.9–235.8 °C; <sup>1</sup>H NMR (DMSO-*d*<sub>6</sub>/300 MHz) 12.7 (br s, 1H), 8.50 (d, *J* = 4.5 Hz, 2H), 7.50 (d, *J* = 8.4 Hz, 2H), 7.32 (m, 4H), 7.10 (m, 4H), 4.23 (s, 2H), 3.08 (m, 2H), 2.79 (m, 2H). ESHRMS *m/z* 387.1417 (M + H, C<sub>23</sub>H<sub>19</sub>ClN<sub>4</sub> requires 387.1376). Anal. (C<sub>23</sub>H<sub>19</sub>ClN<sub>4</sub>) C, H, N.

**1-[3-(4-Chlorophenyl)-4-pyridin-4-yl-1H-pyrazol-5-yl]decahydroisoquinoline (16).** This compound was prepared using the methods described in the synthesis of **4**, **10**, and **11**. mp 226.7–228.0 °C; <sup>1</sup>H NMR (DMSO-*d*<sub>6</sub>/300 MHz) 12.6 (br s, 1H), 8.44 (dd, *J* = 4.8 Hz and *J* = 1.6 Hz, 2H), 7.4–7.2 (br m, 4H), 2.96 (m, 3H), 0.7–1.8 (br m, 13H). ESHRMS *m/z* 393.1842 (M + H, C<sub>23</sub>H<sub>25</sub>ClN<sub>4</sub> requires 393.1846). Anal. (C<sub>23</sub>H<sub>25</sub>ClN<sub>4</sub>) C, H, N.

**1-[3-(4-Chlorophenyl)-4-pyridin-4-yl-1H-pyrazol-5-yl]piperidin-3-ol (17).** This compound was prepared using the methods described in the synthesis of **4**, **10**, and **11**. mp 233.9–234.4 °C; <sup>1</sup>H NMR (DMSO-*d*<sub>6</sub>/300 MHz) 12.6 (br s, 1H), 8.45 (dd, *J* = 4.5 Hz and *J* = 1.5 Hz, 2H), 7.47 (d, *J* = 7.8 Hz, 2H), 7.28 (m, 4H), 4.68 (d, *J* = 4.5 Hz, 1H), 3.55 (m, 1H), 3.22 (br d, *J* = 8.7 Hz, 1H), 2.99 (br d, *J* = 11.7 Hz, 1H), 2.37 (m, 1H), 1.85 (m, 1H), 1.60 (m, 1H), 1.47 (m, 1H), 1.18 (m, 1H). ESHRMS *m/z* 355.1324 (M + H, C<sub>19</sub>H<sub>19</sub>N<sub>4</sub>O requires 355.1326). Anal. (C<sub>19</sub>H<sub>19</sub>ClN<sub>4</sub>O) C, H, N.

**1-[3-(4-Chlorophenyl)-4-pyridin-4-yl-1H-pyrazol-5-yl]piperidin-4-ol (18).** This compound was prepared using the methods

described in the synthesis of **4**, **10**, and **11**. mp 268.8–268.9 °C; <sup>1</sup>H NMR (DMSO-*d*<sub>6</sub>/300 MHz) 12.6 (br s, 1H), 8.45 (d, *J* = 6.0 Hz, 2H), 7.40 (d, *J* = 8.4 Hz, 2H), 7.30 (m, 4H), 4.65 (br d, *J* = 4.2 Hz, 1H), 3.55 (m, 1H), 3.11 (br d, *J* = 12.6 Hz, 2H), 2.65 (dd, *J* = 9.9 Hz and *J* = 10.5 Hz, 2H), 1.73 (d, *J* = 10.2 Hz, 2H), 1.44 (m, 2H). ESHRMS *m/z* 355.1329 (M + H, C<sub>19</sub>H<sub>19</sub>N<sub>4</sub>ClO requires 355.1326). Anal. (C<sub>19</sub>H<sub>19</sub>ClN<sub>4</sub>O) C, H, N.

**(8aS)-2-[3-(4-Chlorophenyl)-4-pyridin-4-yl-1H-pyrazol-5-yl]-octahydropyrrolo[1,2-*a*]pyrazine (19)**. This compound was prepared using the methods described in the synthesis of **4**, **10**, and **11**. mp 226.1–228.8 °C; <sup>1</sup>H NMR (DMSO-*d*<sub>6</sub>/400 MHz) 12.6 (br s, 1H), 8.44 (dd, *J* = 5.6 Hz and *J* = 1.6 Hz, 2H), 7.43 (br d, *J* = 7.2 Hz, 2H), 7.25 (d, *J* = 8.4 Hz, 2H), 7.22 (d, *J* = 5.6 Hz, 2H), 3.21 (d, *J* = 11.2 Hz, 1H), 3.02 (d, *J* = 11.6 Hz, 1H), 2.92 (t, *J* = 7.6 Hz, 1H), 2.85 (d, *J* = 10.8 Hz, 1H), 2.69 (m, 1H), 2.40 (m, 1H), 2.14 (m, 1H), 2.02 (m, 2H), 1.61 (m, 3H), 1.21 (m, 1H). ESHRMS *m/z* 380.1589 (M + H, C<sub>21</sub>H<sub>22</sub>ClN<sub>5</sub> requires 380.1642). Anal. (C<sub>21</sub>H<sub>22</sub>ClN<sub>5</sub>) C, H, N.

**1-[5-(4-Chlorophenyl)-4-pyridin-4-yl-1H-pyrazol-3-yl]-3-methylpiperazine (20)**. This compound was prepared using the methods described in the synthesis of **4**, **10**, and **11**. mp 233.4–234.7 °C; <sup>1</sup>H NMR (DMSO-*d*<sub>6</sub>/400 MHz) 8.4 (d, *J* = 8 Hz, 2H), 7.4 (d, *J* = 11 Hz, 2H), 7.23–7.27 (m, 4H), 3.3 (m, 2H), 2.9 (m, 1H), 2.7 (m, 2H), 2.5 (m, 1H), 2.2 (m, 1H), 0.85 (d, *J* = 8.8 Hz, 3H). Anal. (C<sub>19</sub>H<sub>20</sub>ClN<sub>5</sub>+1.3% H<sub>2</sub>O) C, H: calcd, 6.04; found, 5.52, N.

**1-[5-(4-Chlorophenyl)-4-pyridin-4-yl-1H-pyrazol-3-yl]-3,5-dimethylpiperazine (21)**. This compound was prepared using the methods described in the synthesis of **4**, **10**, and **11**. mp 226.5–228.1 °C; <sup>1</sup>H NMR (DMSO-*d*<sub>6</sub>/400 MHz) 8.4 (d, *J* = 7.6 Hz, 2H), 7.4 (m, 2H), 7.3 (m, 4H), 3.3 (m, 2H), 2.9 (m, 2H), 2.8 (m, 2H), 0.8 (d, *J* = 8.4 Hz, 6H). Anal. (C<sub>20</sub>H<sub>22</sub>ClN<sub>5</sub>) C, H, N.

**p38 Enzyme Assay.** p38 $\alpha$  kinase activity was determined by monitoring the phosphorylation of epidermal growth factor peptide (EGFRP) in the presence of [ $\gamma$ -<sup>33</sup>P]ATP as described previously.<sup>33</sup> Reaction mixtures included 25 mM HEPES pH 7.5, 200  $\mu$ M EGFRP, and 50  $\mu$ M ATP (this concentration represents *K*<sub>m</sub> levels for ATP). Reactions were initiated by the addition of 10–20 nM p38 $\alpha$  previously activated with GST\_MKK6 (p38 $\alpha$ :MKK6, 100:1) for 1 h at 30 °C in the presence of 50  $\mu$ M ATP. Compounds were tested over the range of 0.001  $\mu$ M to 100  $\mu$ M in 10% DMSO. Reactions proceeded for 60 min and were terminated using Dowex resin.

**Acknowledgment.** Diffraction data for the inhibitor complexes were collected at IMCA-CAT beamline 17-ID at the Advanced Photon Source. Use of the IMCA-CAT beamline 17-ID at the Advanced Photon Source was supported by the companies of the Industrial Macromolecular Crystallography Association through a contract with the Center for Advanced Radiation Sources at the University of Chicago. Use of the Advanced Photon Source was supported by the U.S. Department of Energy, Office of Science, Office of Basic Energy Sciences, under Contract No. W-31-109-Eng-38.

**Supporting Information Available:** Combustion analysis data. This material is available free of charge via the Internet at <http://pubs.acs.org>.

## References

- Cohen P. The search for physiological substrates of MAP and SAP kinases in mammalian cells. *Trends Cell Biol.* **1997**, *7*, 353–361.
- Widmann, C.; Gibson, S.; Jarpe, M. B.; Johnson, G. L. Mitogen-activated protein kinase: Conservation of a three-kinase module from yeast to human. *Physiol. Rev.* **1999**, *79*, 143–180.
- Ono, K.; Han, J. The p38 signal transduction pathway: activation and function. *Cell Signal.* **2000**, *12*, 1–13.
- Johnson, G. L.; Lapadat, R. Mitogen-activated protein kinase pathways mediated by ERK, JNK, and p38 protein kinases. *Science* **2002**, *298*, 1911–1912.
- English, J. M.; Cobb, M. H. Pharmacological inhibitors of MAPK pathways. *Trends Pharmacol. Sci.* **2002**, *23*, 40–45.
- Adams, J. L.; Badger, A. M.; Kumar, S.; Lee, J. C. p38 MAP kinase: molecular target for the inhibition of pro-inflammatory cytokines. *Prog. Med. Chem.* **2001**, *38*, 1–60.
- Cirillo, P. F.; Pargellis, C.; Regan, J. The non-diaryl heterocycle classes of p38 MAP kinase inhibitors. *Curr. Top. Med. Chem.* **2002**, *2*, 1021–1035.
- Jackson, P. F.; Bullington, J. L. Pyridinylimidazole based p38 MAP kinase inhibitors. *Curr. Top. Med. Chem.* **2002**, *2*, 1011–1020.
- Lee, J. C.; Kumar, S.; Griswold, D. E.; Underwood, D. C.; Votta, B. J.; Adams, J. L. Inhibition of p38 MAP kinase as a therapeutic strategy. *Immunopharmacology* **2000**, *47*, 185–201.
- Haddad, J. J. VX-745, Vertex Pharmaceuticals. *Curr. Opin. Invest. Drugs* **2001**, *2* (8), 1070–1076.
- Manuscript in preparation.
- Substituted pyrazoles as p38 kinase inhibitors. *Expert Opin. Ther. Pat.* **1999**, *9* (7), 975–979.
- Lieber, E.; Orłowski, R. C. Hydrazinolysis of 1-(Alkylthio)thio-piperidine. *J. Org. Chem.* **1957**, *22*, 88–89.
- Nomoto, Y.; Haruki, T.; Hirata, T.; Teranishi, M.; Ohno, T.; Kubo, K. Studies on Cardiotonic agents V. Synthesis of 1-(6,7-dimethoxy-4-quinazoliny) piperidine. Derivatives carrying various 5-membered heterocyclic rings at the 4-position. *Chem. Pharm. Bull.* **1991**, *39*, 86–90.
- Anantanarayan, A.; Clare, M.; Collins, P. W.; Crich, J. Z.; Devraj, R. V.; Flynn, D. L.; Geng, L.; Graneto, M. J.; Hanau, C. E.; Hanson, G. J.; Hartmann, S. J.; Hepperle, M.; Huang, H.; Khanna, I. K.; Koszyk, F. J.; Liao, S.; Metz, S.; Partis, R. A.; Perry, T. D.; Rao, S. N.; Selness, S. R.; South, M. S.; Stealey, M. A.; Talley, J. J.; Vazquez, M. L.; Weier, R. M.; Xu, X.; Yu, Y. Preparation of heteroarylpyrazoles as p38 kinase inhibitors. PCT Int. Appl. WO0031063A1, 2000.
- Pfeiffer, W. D.; Dilk, E.; Bulka, E. Reaction of 2,4-dimethylthiosemicarbazide with alpha-halo ketones. *Z. Chem.* **1977**, *175*, 173–4.
- Apparao, S.; Ila, H.; Junjappa, H. A new, general synthesis of 1-substituted 2-amino-4-aryl-5-methylthiopyrroles using alpha-ketoketene S, S-acetals. Part 14. *Synthesis* **1981**, *1*, 65–66.
- Katagiri, N.; Ise, S.; Watanabe, N.; Kaneko, C. Cycloadditions in syntheses. XLVIII. Synthesis of nucleosides and related compounds. XVII. Dialkyl 1,3-dithiathan- and 1,3-dithiolan-2-ylidene malonate S-oxides: equivalents to dialkoxycarbonylketenes. *Chem. Pharm. Bull.* **1990**, *38*, 3242–3248.
- Hanks, S. K.; Quinn, A. M.; Hunter, T. The protein kinase family: conserved features and deduced phylogeny of the catalytic domain. *Science* **1988**, *241*, 42–52.
- García-Sosa, Alfonso, T.; Mancera, Ricardo, L.; Dean, Phillip, M. WaterScore: a novel method for distinguishing between bound and displaceable water molecules in the crystal structure of the binding site of protein-ligand complexes. *J. Mol. Model.* **2003**, *9*, 172–182.
- Lam, Patrick, Y.; Jadhav, Prabhakar, K.; Eyermann, Charles, J.; Hodge, C. Nicholas; Ru, Yu; Bachelier, Lee T.; Meek, J. L.; Otto, Michael J.; Rayner, Marlene M. Rational design of potent, bioavailable, nonpeptide cyclic ureas as HIV protease inhibitors. *Science* **1994**, *263*, 380–384.
- Finley, James, B.; Atigadda, Venkatram, R.; Duarte, Franco; Zhao, James, J.; Brouillette, Wayne, J.; Air, Gillian, M.; Luo, Ming. Novel Aromatic Inhibitors of Influenza Virus Neuraminidase Make Selective Interactions with Conserved Residues and Water Molecules in the Active Site. *J. Mol. Biol.* **1999**, *293*, 1107–1119.
- Zaslavsky, Boris; Gulyaeva, Nellie; Zaslavsky, Alexander; Lechner, Pamela; Chlenov, Michael; Chait, Arnon. Relative hydrophobicity and lipophilicity of Beta-blockers and related compounds as measured by aqueous two-phase partitioning, octanol-buffer partitioning, and HPLC. *Eur. J. Pharm. Sci.* **2002**, *17*, 81–93.
- Walters, Patrick, W.; Murcko, Ajay; Murcko, Mark, A. Recognizing molecules with drug-like properties. *Curr. Opin. Chem. Biol.* **1999**, *3*, 384–387.
- Lipinski, Christopher, A.; Lombardo, Franco; Dominy, Beryl, W.; Feeney, Paul, J. Experimental and computational approaches to estimate solubility and permeability in drug discovery and developmental settings. *Adv. Drug Delivery Rev.* **1997**, *23*, 3–25.
- Wilson, K. P.; McCaffrey, P. G.; Hsiao, K.; Pazhanisamy, S.; Galullo, V.; Bemis, G. W.; Fitzgibbon, M. J.; Caron, P. R.; Murcko, M. A.; Su, S. S. The structural basis for the specificity of pyridinylimidazole inhibitors of p38 MAP kinase. *Chem. Biol.* **1997**, *4*, 423–431.
- Wang, Z.; Canagarajah, B. J.; Boehm, J. C.; Kassisa, S.; Cobb, M. H.; Young, P. R.; Abdel-Meguid, S.; Adams, J. L.; Goldsmith, E. J. Structural basis of inhibitor selectivity in MAP kinases. *Structure* **1998**, *6*, 1117–1128.
- Stuart, J. M.; Townes, A. S.; Kang, A. H. Collagen autoimmune arthritis. *Ann. Rev. Immunol.* **1984**, *2*, 199–218.

- (29) Perretti, M.; Duncan, G. S.; Flower, R. J.; Peers, S. H. Serum corticosterone, interleukin-1 and tumor necrosis factor in rat experimental endotoxemia: Comparison between Lewis and Wistar strains. *Br. J. Pharmacol.* **1993**, *110*, 868–874.
- (30) Staines, N. A.; Wooley, P. H. Collagen arthritis—what can it teach us? *Br. J. Rheum.* **1994**, *33*, 798–807.
- (31) Badger, A. M.; Bradbeer, J. N.; Votta, B.; Lee, J. C.; Adams, J. L.; Griswold, D. E. Pharmacological profile of SB 203580, a selective inhibitor of cytokine suppressive binding protein/p38 kinase, in animal models of arthritis, bone resorption, endotoxin shock and immune function. *J. Pharmacol. Exp. Ther.* **1996**, *279*, 1453–1461.
- (32) Thorbecke, G. J.; Shah, R.; Leu, C. H.; Kuruvilla, A. P.; Hardison, A. M.; Palladino, M. A. Involvement of endogenous tumor necrosis factor alpha and transforming growth factor beta during induction of collagen type II arthritis in mice. *Proc. Natl. Acad. Sci. U.S.A.* **1992**, Aug 15, *89* (16), 7375–9.
- (33) Mbalaviele, G.; Anderson, G. A.; Jones, A.; De Ciechi, P.; Settle, S.; Mních, S.; Thiede, M.; Abu-Amer, Y.; Portanova, J.; Monahan, J. Inhibition of p38 Mitogen-Activated Protein Kinase Prevents Inflammatory Bone Destruction. *J. Pharmacol. Exp. Ther.* **2006**, *317*, 1044–1053.

JM0611915